Tuning of energy storage capacity of $BiFeO_3$ nanoparticles By La/Cr co-doping

M. Amin[a], G. M. Mustafa[b *], Anwar-ul-Haq[a], B. Younas[a], M. I. Khan[a], M. Atif[c], A. Ashraf[d], M. Ali[e]
[a]*Department of Physics, The University of Lahore, Lahore, Pakistan*
[b]*Department of Physics, Division of Science & Technology, University of Education, Lahore, Pakistan*
[c]*Department of Physics and Astronomy, College of Science, King Saud University, P O Box 2455, Riyadh 11451, Saudi Arabia*
[d]*Departamento de Engenharia de Materiais, Escola de Engenharia de Lorena (EEL), Universidade de São Paulo (USP), Lorena 12.612 - 550, Sao Paulo, Brazil*
[e]*The University of Electro-Communications Tokyo Japan*

Cr-doped $Bi_{0.9}La_{0.1}Fe_{1-x}Cr_xO_3$ with x = 0, 0.05, 0.10, 0.15, and 0.20 is fabricated by the sol-gel auto-combustion. The rhombohedral phase of pure and doped bismuth ferrite is confirmed during structural analysis. The structural parameters are further refined using X'pert High score plus by calculating the atomic positions and different profile factors which assured the reliability of the structural data. As Cr content is increased, it results the better crystallinity with uniform distribution of multi-shape grains. The size of grains varied which affected the microstructural characteristics of the parent compositions. The presence of constituent elements with a stoichiometric ratio is established by elemental analysis which guarantees elemental purity of prepared samples. The introduction of La followed by increasing contents of Cr in the parent composition improved the magnetic response. Ferroelectric analysis revealed that both saturation and remanent polarizations are increased with increasing doping levels. The calculation of recoverable and energy loss density ensured that the parent composition was more suitable for the energy storage devices. The multiferroic properties of synthesized samples are comprehensively explored to evaluate the worth of these materials for futuristic energy storage and multistate devices.

(Received May 14, 2024; Accepted September 20, 2024)

Keywords: Magneto-electric multiferroics, Nanoparticles, Rietveld's refinement, Energy storage efficiency, Recoverable and energy loss densities

1. Introduction

The materials having one or more basic ferroic orders in the single phase are called multiferroic materials and these materials grabbed a huge interest of the scientific community due to their multifunctional response to upcoming innovative devices. These materials include, ferroelectric, ferromagnetic, ferroelastic, and ferrotoroidic which are considered as a building block for next-generation smart, efficient, and sophisticated devices. Magnetoelectric materials are a subclass of multiferroic materials that display ferroelectric and ferromagnetic behaviors simultaneously and have the potential to revolutionize advanced multistate devices [1]. Since the origin of ferroelectricity and ferromagnetism are exclusive, therefore their simultaneous coexistence in a single phase is a miracle. Among different available materials where there is a possibility of coexisting of mutually excluding phenomenon of ferroelectricity and ferromagnetism, bismuth ferrite $BiFO_3$ (BFO) is at the top of the list. It is the sole member of the multiferroic family to date which exhibits magnetoelectric (ME) coupling above the room temperature. Investigation of magnetic and ferroelectric features of BFO exposed G-type anti-ferromagnetic character (AFM) with Neel temperature of 1103 K and inherent ferroelectric character with a Curie temperature of 643 K. This big difference among magnetic and ferroelectric

* Corresponding authors: gmmustafa25@gmail.com
https://doi.org/10.15251/JOR.2024.205.651

ordering temperatures is responsible for the weak linear ME coupling in BFO. Further, BFO belongs to space group R3c with a spiral spin structure that rotates within the crystal covering a distance equal to 62 nm which further decreases its magnetic behavior [2-4]. The space-modulated spiral spin structure can be controlled by (i) making BFO thin films, (ii) replacing Bi in BFO with rare earth elements or (iii) applying a strong magnetic field [5]. Therefore, there is an urgent need to optimize both ferroelectric and magnetic phenomena to make BFO feasible for ME devices. Researchers across the globe always tried to develop low-cost, time-efficient, sophisticated devices with low energy consumption and BFO with multiferroic response that meet all these salient features and therefore have the potential for technologically innovative devices.

So far, BFO is not commercialization owing to the weak magnetoelectric coupling therefore untired efforts have been devoted by researchers to enhance the ME coupling and reduce derivatives by the controlled tuning of microstructures through suitable single and co-doping in BFO. For example, Atiq *et al*. 2019 [6] investigated the magnetoelectric response of La-substituted $BiFeO_3$ and proposed that these materials are suitable for spintronic-based sensing and data-storing devices. Verma devoted a full chapter to the synthesis and multiferroic characteristics of $BiFeO_3$ and covered various approaches required to enhance the magnetoelectricity in $BiFeO_3$ to make them feasible for data storage devices [7]. Khan *et al*. evaluated the effect of the substitution of Mn in $BiFeO_3$ on the magneto-resistive response of these compositions and their role in low-field sensors [8]. Bousquet and Cano working jointly realized that non-linear magnetic ordering in perovskites is linked with their multiferroicity [9]. In addition, Amirov *et al*. [5] noticed that La/Nd co-doping improved magnetic and electromagnetic interaction in BFO bulk ceramics. Furthermore, La substitution stabilized the rhombohedral phase of BFO, reduced oxygen vacancies, and abated leakage current which are the main issues to be addressed before its commercialization. Likewise, Baettig and Spaldin mentioned that the substitution of Fe^{3+} in BFO at Fe^{3+} sites results in an improvement in the magnetism of BFO which is credited to the robust super-exchange interaction between Fe^{3+} and Cr^{3+} ions [10]. Similarly, the substitution of Cr in BFO on the morphology, dielectric, magnetic, and leakage current has been comprehensively studied by Murari *et al*. [11]. This comprehensive literature review motivated us enough to explore the morphological, ferroelectric, and magnetic behavior of $BiFeO_3$ modulated by La and Cr co-doping. We believe that this work would be interesting and provide a better insight into the doping-driven multifunctional response of $BiFeO_3$. The next work in this communication has been summarized as follows; experimental details are given in section 2; the results and discussion have been done in section 3 while the conclusion is described in section 4.

2. Experimental details

Sol-gel auto-combustion is one of the facile chemical routes that is extensively being used to synthesize a variety of chemical compounds at the lab scale because of its cost-effectiveness and time-efficient features. In addition, it does not require any sophisticated instrument to execute the process. In the current study, we fabricated the La and Cr co-doped BFO nanoparticles with the formula $Bi_{0.9}La_{0.1}Fe_{1-x}Cr_xO_3$ (x = 0, 0.05, 0.10, 0.15, and 0.20) and for this synthesis the analytical graded bismuth nitrate pentahydrate [Bi $(NO_3)_2.5H_2O$, Sigma Aldrich 99.9%], iron nitrate nonahydrate [$Fe(NO_3)_3.9H_2O$, Sigma Aldrich 99.9%], lanthanum nitrate [$La(NO_3)_3$, Merc 99.9%] and Chromium nitrate [$Cr(NO_3)_3$, Merc 99.9%] were utilized as precursors. To assist self-ignition and to accelerate the combustion process, the chelating agent's urea and glycine were used to get purified output. The stoichiometric amounts of all precursors were calculated and dissolved deionized (DI) water because bismuth nitrate is easily soluble thus dissolution of $Bi(NO_3)_2.5H_2O$ was assisted with 3M HNO_3 solution. The solution of $Bi(NO_3)_2.5H_2O$ was heated and stirred with a dropwise addition of HNO_3 solution until the milky solution became transparent. Then precursors and chelating agent's solutions were decanted into a beaker and that beaker was placed on the hot plate at 110 °C with nonstop stirring with the help of a stirrer. The constant stirring and heating turned the solution into a dark viscous dense gel form. At this stage, the temperature was immediately augmented to 350 °C. This considerable temperature was enough to trigger the chelating agents to catch fire causing auto-combustion. Due to the auto-combustion, the

temperature inside the beaker suddenly raised to promote the exotic exothermic reaction and liberated several gases. After combustion, the residual was ground using mortar and pestle followed by calcination at 550°C for 3 h. The detail of the synthesis summary is provided in Figure 1. All the samples were synthesized using the same methodology. The final powder form was used to make pellets of thickness 1-1.1 mm and diameter 10 mm. Finally, samples were sintered for 1h at 400°C to eliminate the residual gases.

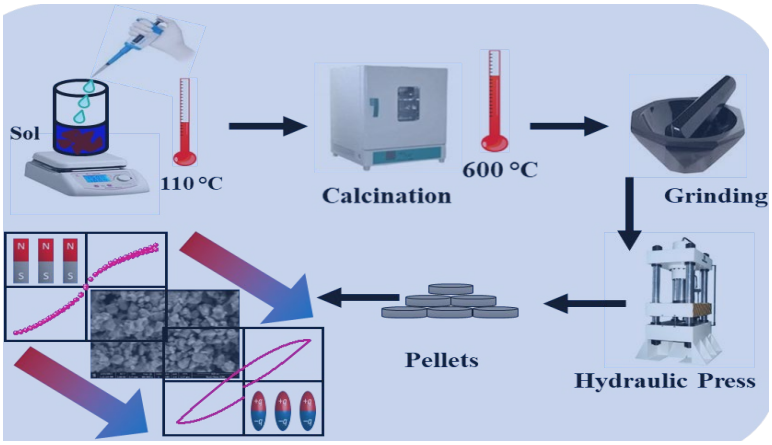

Fig. 1. Stepwise synthesis summary of the prepared samples.

The phase purity and crystalline nature were analyzed by X-ray diffractometer of Rigaku D/MAXIIA, whereas surface morphology and elemental purity were judged by Nova-Nano SEM 450. An energy-dispersive X-ray spectroscope was used to ensure the formation of exact composition in accordance with the stochiometric formula. To explore the ferroelectric behavior, a precision multiferroic tester was used whereas magnetic investigations were carried out by Lakeshore 7404 vibrating sample magnetometer (VSM).

3. Results and discussion

3.1. Structural and phase analysis

To analyze the crystal structure of BFO NPs, data obtained from an X-ray diffractometer was refined using X'pert HighScore Plus [12]. X'pert HighScore Plus is one of the reliable software that is utilized for the analysis of crystal structure. To refine the crystal structure of any composition, first of all, its diffracted data is uploaded into the software. Then, the crystallographic information file (CIF) of the same composition as a standard file is uploaded with the required space group. After that, these two files are matched to evaluate the credibility of newly synthesized samples. The Rietveld refined XRD graphs of undoped and doped BFO compositions are presented in Figure 2. These Figures contain the experimental data, standard data, and difference plots. The crystallographic information file (CIF) # 1001090 was used in the present case as a standard data file. These graphs exhibited that neither pure nor doped BFO contained any secondary phase and thus confirmed the formation of impurity-free BFO with space group R3c. This software quantifies the matching between given and standard data in terms of residual factors termed profile factor (R_p), weighted profile factor (R_{wp}), and expected profile factor (R_{exp}). These parameters help to determine the goodness of fit (GoF) which is the ultimate parameter to determine the credibility of the material. The measured values of all these profile factors in addition to lattice parameters are listed in Table 1. The ionic radii of Fe^{3+} and Cr^{3+} are 0.645 and 0.615Å, therefore, this substitution leads to unit cell shrinkage due to which unit cell volume is decreased. It is evident from these figures that both a and c decreased such that c/a remains almost constant which established the successful replacement of La at Bi and Cr at Fe site in the BFO [3].

The density calculation revealed that $Bi_{0.9}La_{0.1}Fe_{0.80}Cr_{0.20}O_3$ composition has the highest density. The crystallite size was measured by the Scherrer formula which increased with increasing Cr contents up to 0.15 and decreased when Cr is further increased to 0.20.

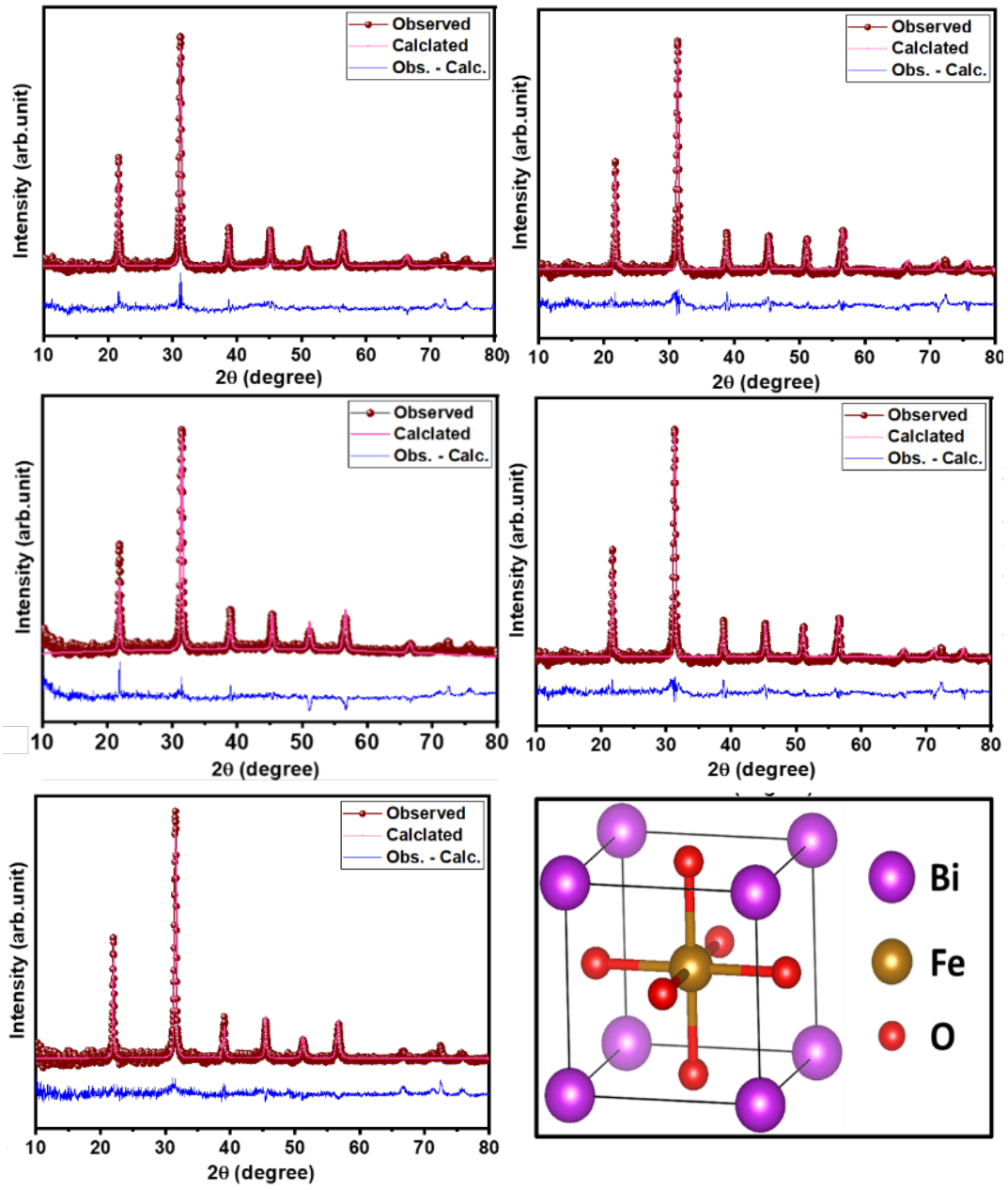

Fig. 2. Rietveld refined X-ray diffraction patterns of La/Cr co-doped $BiFeO_3$ and rhombohedral unit cell of pure $BiFeO_3$.

Owing to the strong dependence of the ferroelectric behavior of BFO with the tilting of the octahedron, the bond length and bond angles were also recorded during refinement which are presented in Table 2. BFO crystal structure contains an oxygen octahedra (FeO_6) network in which Fe^{3+} ions lie at octahedral voids with three short degenerate and three long degenerate bond lengths. The incorporation of 10% La at Bi-site results in the deformation of bond angle and bond length of FeO_6 octahedra. This modification in structural parameters is thermodynamically favorable which lowers the energy of the system. This lower energy makes the system more stable.

The doping of La^{3+} with ionic radius 1.16Å at the place of Bi^{3+} with ionic radius 1.17Å brings the change in crystal structure in several ways it reduces long-range ferroelectric ordering persists due to lone pair of Bi and reduces the distance between cations of octahedron [13, 14]. This kind of structural modification can significantly affect the ferroelectric as well as magnetic response of the material.

Table 1. Rietveld's refined structural parameters of $Bi_{0.9}La_{0.1}Fe_{1-x}Cr_xO_3$ (x = 0, 0.05, 0.10, 0.15 & 0.20).

Parameters	x = 0.00	x = 0.05	x = 0.10	x = 0.15	x = 0.20
$a = b$ (Å)	5.58	5.55	5.51	5.49	5.45
c (Å)	13.86	13.79	13.76	13.71	13.67
D (nm)	17.9	27.3	33.5	37.3	25.7
ρ (g/cm^3)	8.40	8.43	8.43	8.45	8.49
R_p	9.15	11.45	26.51	15.65	16.04
R_{wp}	10.245	13.542	29.57	17.658	18.65
D_{stats}	0.12	0.08	0.009	0.16	0.19
GoF	1.59	1.61	3.31	2.11	2.34

Table 2. Bond type and length for $Bi_{0.9}La_{0.1}Fe_{1-x}Cr_xO_3$ (x = 0, 0.05, 0.10, 0.15 & 0.20).

Composition	Bond Type	Bond length (Å)
x = 0.00	Bi/La1 - O1	2.33
	Bi/La - Fe	3.05
	Fe - O1	1.94
x = 0.05	Bi/La- Fe/Cr	3.03
	Bi/La - O	2.29
	Fe/Cr - O	1.93
x = 0.10	Bi/La- Fe/Cr	3.04
	Bi/La – O	3.19
	Fe/Cr - O	1.93
x = 0.15	Bi/La –Fe/Cr	3.05
	Bi/La – O	2.30
	Fe/Cr - O	1.93
x = 0.20	Bi/La – Fe/Cr	3.31
	Bi/La – O	2.31
	Fe/Cr - O	1.93

3.2. Morphological and microstructural analysis

The microstructure of the material substantially influences the material's characteristics. The microstructure analysis of a material involves the measurement of grains and grain boundaries, identification of voids and surface defects, and estimation of the porosity of the material as well. To study the microstructure of the material, the FESEM image of $Bi_{0.9}La_{0.1}Fe_{0.8}Cr_{0.2}O_3$ is presented in Figure 3 at 100,000×. The FESEM images of the rest of the samples can be found in our previous work [15]. From these images, it is easy to find a relation between grain size and La/Cr doping. The FESEM image for x = 0.2, shows a uniformly dispersed microstructure with a slight variation in size. The porosity of samples increased with increasing doping contents which affected the properties of the material significantly. The shrinkage of the size of grains with increasing substitution contents might be ascribed to the decreasing oxygen vacancies that suppress electronic transportation [15-18]. Java-based ImageJ software assisted in measuring grain size which lies in the 8-30 nm range. The presence of holes and voids on the surface is ascribed to the escape of gasses in the sintering process [19]. A little deformation seen on the grain boundaries of all the compositions may be the result of the grinding of powders during the synthesis process of the ceramics [15].

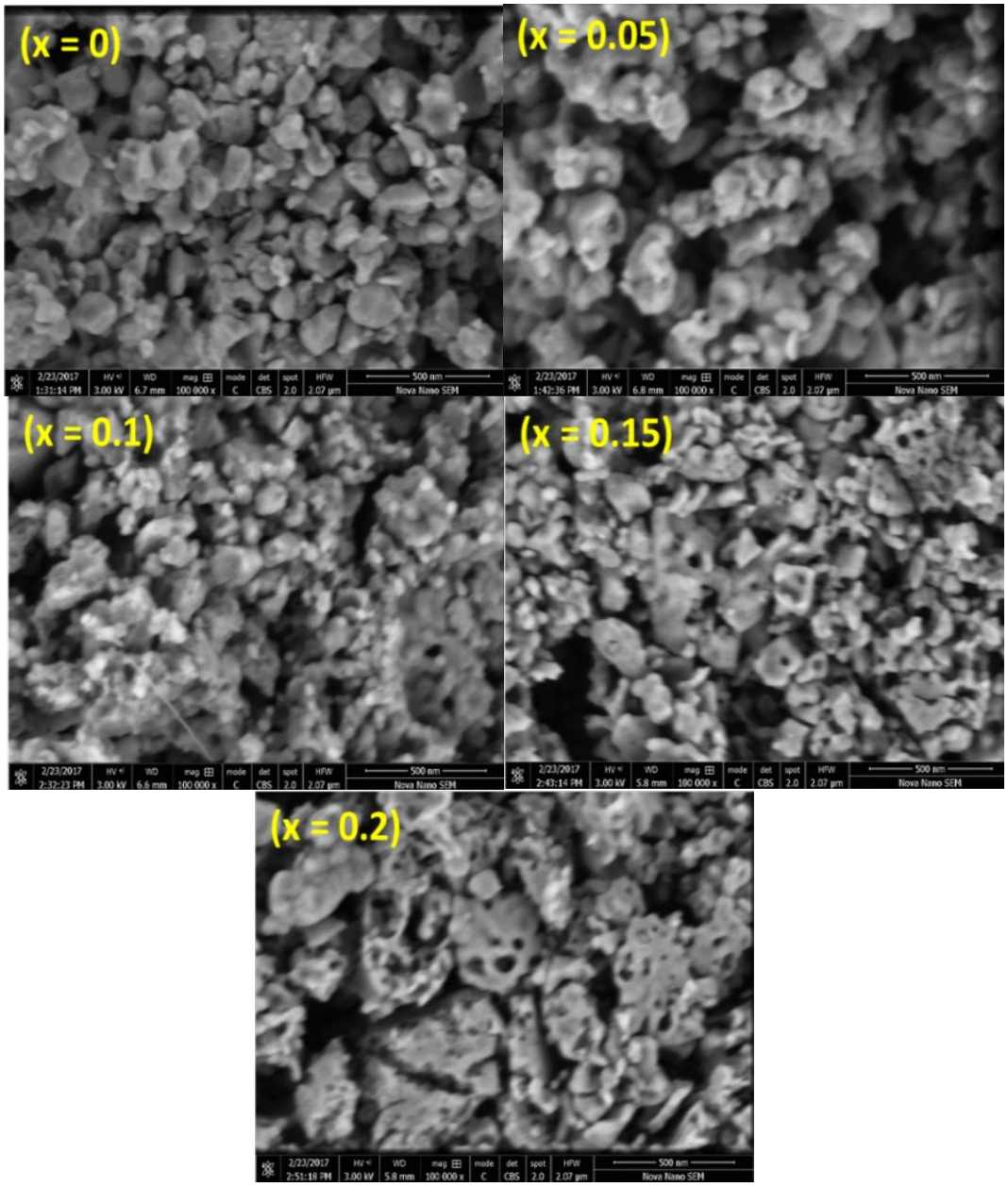

Fig. 3. SEM images of La/Cr co-doped $BiFeO_3$ samples at 100,000×

3.3. Compositional elemental analysis

To detect and quantify different elements present in the composition, EDX analysis is usually employed. Figure 4 shows the EDX spectrum of $Bi_{0.9}La_{0.1}Fe_{0.80}Cr_{0.20}O_3$ assured Bi, La, Fe, Cr, and O existence according to the empirical formula. Since no impurity element is detected in this spectrum, therefore, we can claim that this is an appropriate method to manufacture contamination-free BFO nanoparticles. The atomic and weight percentages of all elements provided by the machine are present in Table 3 which are quite consistent with the empirical formula of these compositions.

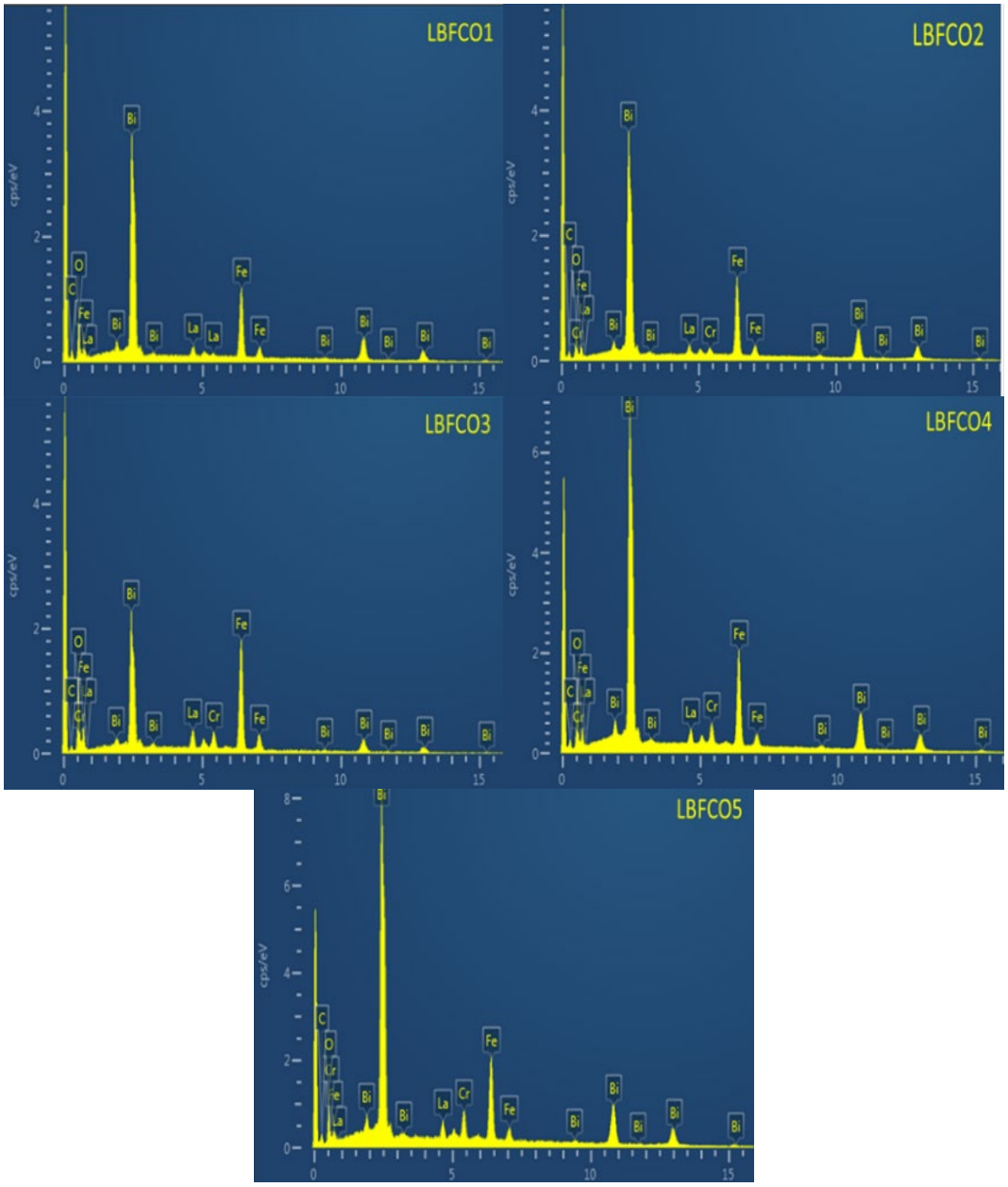

Fig. 4. Energy dispersive X-ray spectra of La/Cr co-doped $BiFeO_3$ samples.

Table 3. Quantitative analysis of each element present in BLFCO samples.

Elements	BLFCO1		BLFCO2		BLFCO3		BLFCO4		BLFCO5	
	wt%	at%	wt%	at%	wt%	at%	wt%	at%	wt%	at%
C	0.8.34	2.58	6.05	1.69	5.02	1.67	5.23	1.72	5.35	1.73
O	18.94	14.06	16.07	11.23	25.98	27.17	18.29	14.96	16.35	12.96
Cr	-	-	0.81	0.79	2.14	2.54	2.15	2.42	3	3.33
Fe	14.95	16.29	17.2	17.72	24.77	29.39	13.78	16.32	12.49	14.61
La	3.78	3.77	3.94	3.7	7.06	8.23	4.16	4.49	4.76	5.07
Bi	53.99	58.68	55.93	56.75	35.02	40.07	56.39	66.43	58.05	67.63
Total	100	100	100	100	100	100	100	100	100	100

3.4. Magnetic analysis

A vibrating sample magnetometer (VSM) was utilized to analyze the magnetic response of these materials and magnetization against magnetic field (M-H) loops of La and Cr co-doped BFO are presented in Figure 5 in the magnetic field range ± 10000 Oe. These loops are quite identical to previously reported results [2, 20, 21], where we can see that magnetization improved with the upsurge of the magnetic field and exhibited the typical anti-ferromagnetic loops. The shape of the MH loop plays a deterministic role regarding the microstructure of the magnetic material which is quantified by the squareness. The squareness ratio (M_r/M_s) is a key term that can be used to distinguish the single domain and multidomain particles [22]. Mostafavi and Ataie [23] stated that for single-grain domains the value of $M_r/M_s > 0.5$ whereas for multidomain grains $M_r/M_s < 0.5$. The measured values of all the magnetic parameters are provided in Table 4. Since M_r/M_s value for all the samples is less than 0.5 it indicates the polycrystalline nature of these materials. The value of magnetization depends upon Cr contents in $Bi_{0.9}La_{0.1}Fe_{1-x}Cr_xO_3$ as can be seen in Table 4. The incorporation of Cr at Fe sites significantly enhanced both M_S and M_r up to Cr = 0.15. The values of these magnetic parameters (M_r and M_s) were decreased when the value of Cr was increased to 0.20. This kind of anomaly in magnetic behavior has been stated in the previous literature [2, 24-26]. These anomalies are credited to the pinning effects that arise from the random dispersal of O vacancies on domain walls [27, 28]. Bhushan *et al*. [29] prepared a series of Ce substituted BFO and observed that the value of M_s increased up to 3% doping of Ce and when this doping concentration was increased to 5%, the value of M_s decreased. A similar behavior was also recorded by Wang *et al*. [25] when they doped Cr in BFO. In addition, Hu *et al*. [2] studied $LaFe_{1-x}Cr_xO_3$ ($0 \leq x \leq 1$) system and noticed that M_s and M_r first increased up to 0.5 and then decreased. Based on these observations, it is perceived that microstructures beyond a particular doping level limit the material's ability to work properly. Several reports are available where the magnetization monotonically increases with increasing contents of Cr [25, 30-35]. Since BFO is very unstable therefore it usually undergoes a structural transformation to different secondary phases like $Bi_2Fe_4O_9$, $Bi_{25}FeO_{40}$, $Bi_{36}Fe_{24}O_{57}$, and Fe_2O_3 and this transformation can significantly contribute magnetic character of material because the secondary phase above mentioned exhibits the magnetic behavior [12, 36, 37]. In the section of Rietveld's refinement, it has been observed that there is no impurity in fabricated samples thus role of secondary phases in magnet behavior is negligibly small. Zhang *et al*. [38] discovered that La substitution in BFO is one of the main causes of nonlinear behavior in the MH loop. Cheng *et al*. [24] described that doping of La at Bi site up to 10% did not influence its magnetic character significantly. In this study, we doped 10% Bi with La and observed a minute variation in the magnetic behavior of BFO, however, when Cr was introduced and its concentration was increased, it substantially modified the magnetic response of the material. These results can be understood based on the connection of the anti-ferromagnetic planes of Fe with the ferromagnetic planes of Cr. The individual magnetic moments of Cr and Fe when combined give rise to the magnetic moment of $2\mu_B$ per Fe-Cr pair due to the high super-exchange interaction which ultimately increases the magnetic response of the material [39]. This increase in magnetic behavior is also associated with the size of NPs. When the size of NPs decreases from 62nm, the G-type helical spin structure is disrupted because there is a helical symmetry of periodicity 62 nm. It converts the helical arrangement of magnetic moments to a straight geometry and thus increases the magnetization. [4, 40-44]. In the present study, particle size lies in the 8-20 nm range as depicted from the FESEM images [15] so it is assisted that the improved magnetic behavior of the present series of samples is due to grain size reduction with increasing doping level of Cr in BFO. This reduction in the grain size yields a high surface-to-volume ratio and presents a wide platform for uncompensated spins at the surface which contribute to high magnetization. With the decrease in grain size, the number of uncompensated spins increases [45]. Since placement of Cr at the Fe site in BFO breaks the canted spiral spin structure of BFO which is another possible reason for the increase in magnetization. As depicted in the structural study, the increasing Cr concentration in BFO reduced the lattice constants "*a*" and "*c*" which resulted in the collapsing and breaking of the canted spin structure of BFO giving an upsurge to magnetization [46]. The titling of FeO_6 octahedron causes the change in bond angle and bond length which is responsible for the active magnetic behavior of these materials [47, 48]. The underlying mechanism behind this response is the "Dzyaloshinsky-Moriya interaction". The

doping of Cr ions in place of Fe ions tailors the crystal structure of BFO that can change the Fe-O-Fe bond angle and intrinsic spin order which results in a homogeneous canted structure from the spatially modulated crystal structure and improves the magnetic response [33].

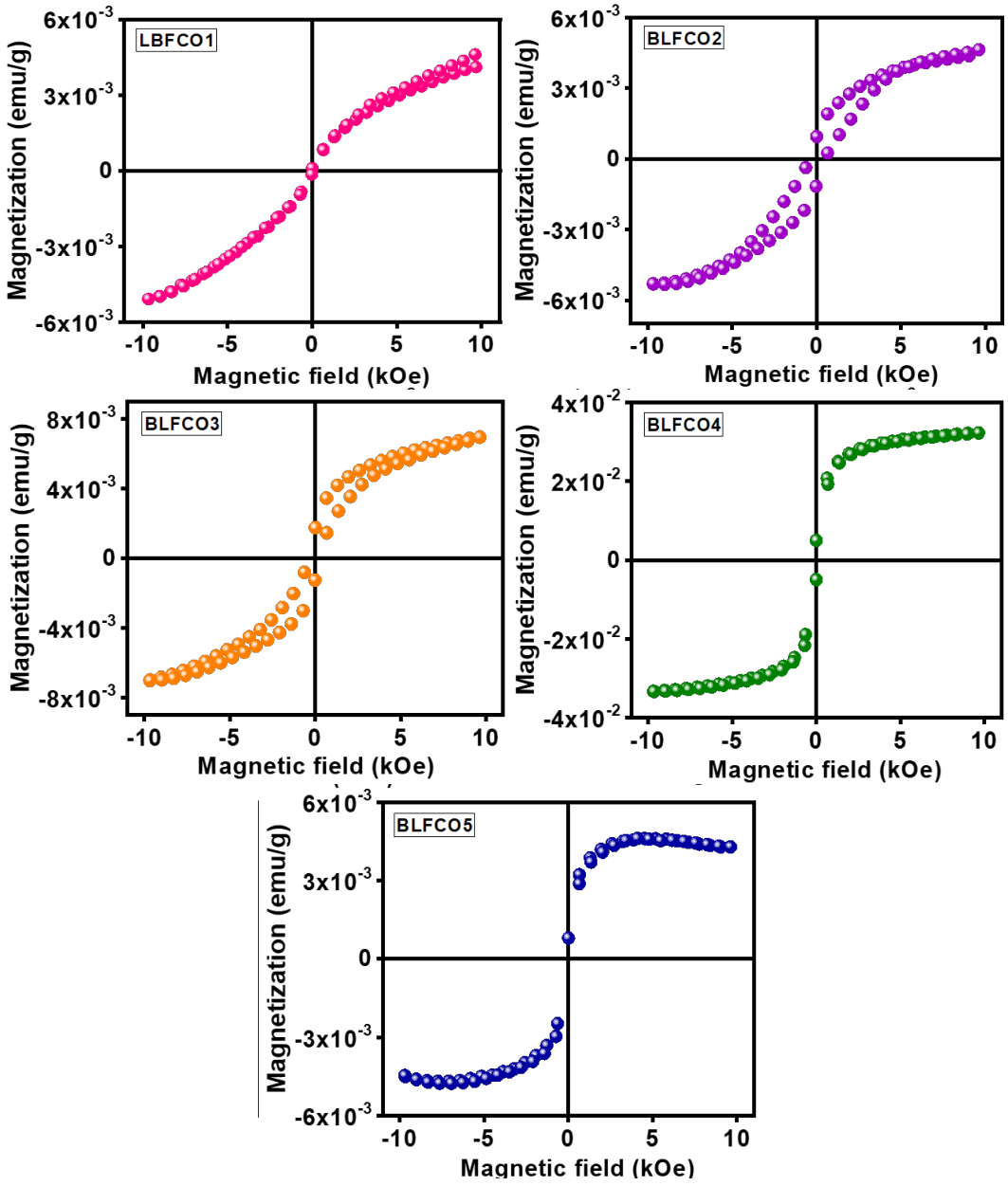

Fig. 5. Magnetization against magnetic field hysteresis loops for La/Cr co-doped $BiFeO_3$.

Table 4. Computed magnetic parameters for $Bi_{0.9}Sr_{0.1}Fe_{1-x}Cr_xO_3$ (x = 0, 0.05, 0.10, 0.15 & 0.20).

Sample Composition	(H_c) (G)	(M_s) (emu/g)	(M_r) (emu/g)	(M_r/M_s)
$La_{0.1}Bi_{0.9}FeO_3$	1.0265	4.843×10^{-3}	106.30×10^{-6}	0.022
$La_{0.1}Bi_{0.9}Fe_{0.95}Cr_{0.05}O_3$	496.99	4.9817×10^{-3}	1.0170×10^{-3}	0.20
$La_{0.1}Bi_{0.9}Fe_{0.90}Cr_{0.10}O_3$	366.83	7.0077×10^{-3}	1.4509×10^{-3}	0.21
$La_{0.1}Bi_{0.9}Fe_{0.85}Cr_{0.15}O_3$	136.84	32.798×10^{-3}	4.9142×10^{-3}	0.15
$La_{0.1}Bi_{0.9}Fe_{0.80}Cr_{0.20}O_3$	114.48	4.6857×10^{-3}	579.32×10^{-6}	0.12

3.5. Ferroelectric analysis

The analysis of PE loops is a typical approach to investigating the ferroelectric response of a material. The PE loops of all compositions are presented in Figure 6. These loops are unsaturated as well as broken along the negative polarization axis and matched well with the previous results [4, 48-50]. Tang *et al*. [49] asserted that high leakage current density is the basic reason behind these broken and unsaturated loops due to electrical breakdown at higher voltage. Similarly, Mukherjee *et al*. [51], described that it is challenging to achieve saturated PE loops of BFO like real ferroelectric material due to the high leakage current exhibited by this ceramic due to its high conductivity and low resistive behavior. This leakage of BFO is one of its notable drawbacks which impede its commercialization. Many authors in the field believe that the realization of PE loops like other true ferroelectric materials is difficult for BFO owing to high leakage current density [4, 52, 53].

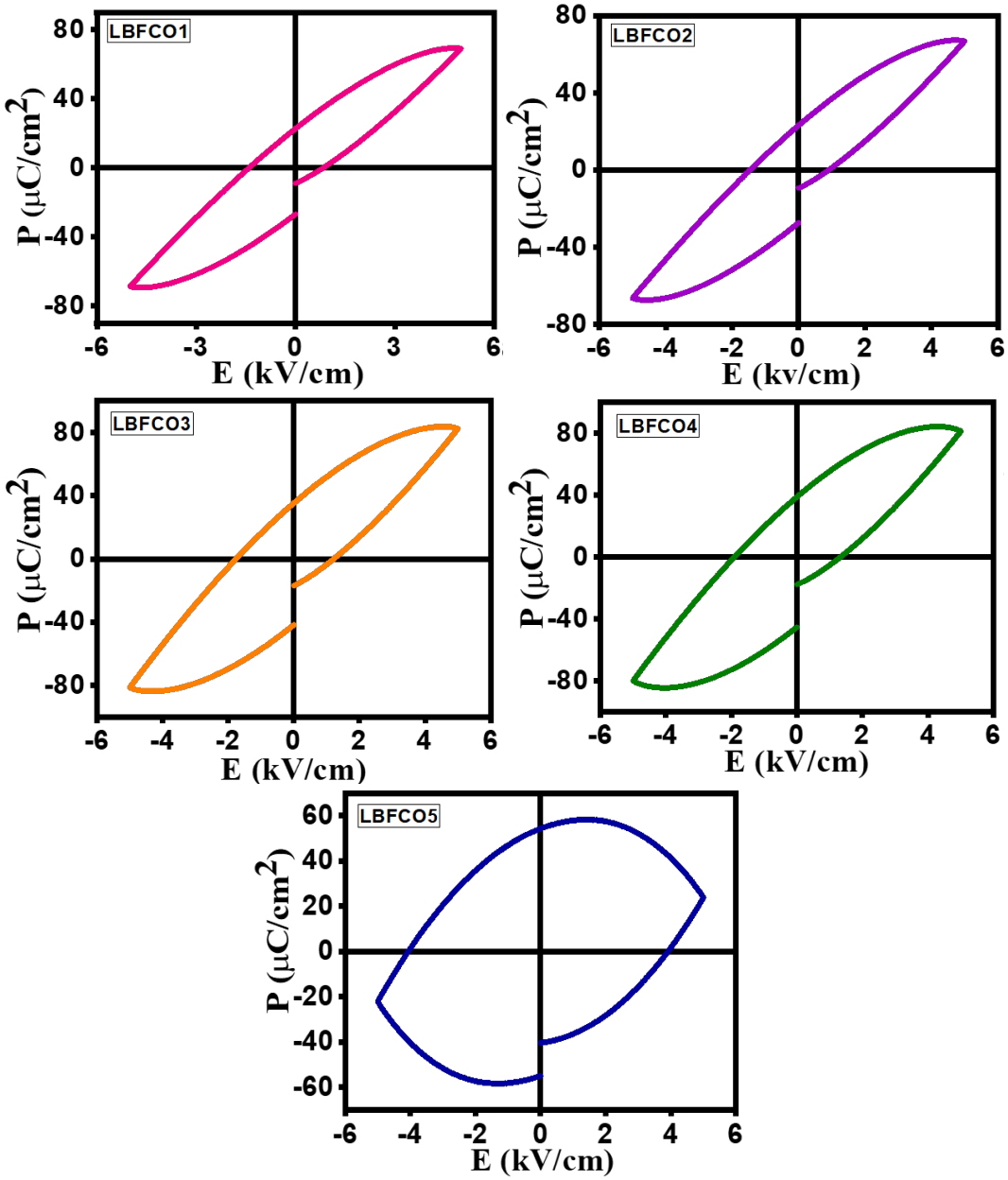

Fig. 6. Polarization versus electric field loops of La/Cr co-doped $BiFeO_3$.

The observed partial saturated PE loops exhibit the ferroelectric and conducting (leaky) behavior of the synthesized compositions. For x =0.20, the PE loop is round and reveals the leakiest behavior among all the samples. For this sample, the maximum value of polarization was noticed as 5.90 × 10^{-4} C/cm^2 at 1.75kV/cm which decreased with further rise in strength of the applied electric field. The starting of the leakage current before the full switching of the electric field is the reason behind this incomplete saturation of polarization [24]. The same results have also been reported in the literature [52, 53]. The roundedness of these PE loops is ascribed to a large leakage current which arises from a number of factors including, low crystallinity, low thickness, imperfections, high absorbency, grain size effect, and cation or anion vacancies [4, 37, 48, 49, 53-56]. Dho *et al.* [57], suggested that the presence of impurity energy levels inside the bandgap of BFO provides a pathway for electronic transition which causes the leakage current in BFO. Some researchers believe that oxygen vacancies are more crucial than Fe^{2+} ions for controlling the leakage current due to which the breakdown voltage is lowered [58, 59]. The excess leakage current may damage the device due to overheating. The ferroelectric behavior is improved with La and Cr doping because loops became slim and smart and measured standards of maximum polarization (P_M), remnant polarization (P_R), and coercive field (E_C) are provided in Table 5 and are plotted in Figure 7(a). The highest value of P_R for x = 0.20 (densest composition with density 8.49 g/cm^3) is noticed as 5.50 × 10^{-4} C/cm^2, which is 24 times higher than the parent composition. The leaky nature of BFO-based ceramics can be minimized by increasing their density. It is asserted that the research community should adopt different approaches to synthesize single crystal and denser microstructures of these materials to improve their ferroelectric behavior [37, 49]. Kumar *et al.* [60] prepared BFO microstructures without secondary phases but saturated P-E hysteresis loops were not observed because of the conducting character and small density of the synthesized samples. An unsaturated and broken P-E loop was exhibited by a less dense BFO composition while a saturated P-E loop was displayed by a denser microstructure of the same material [61].

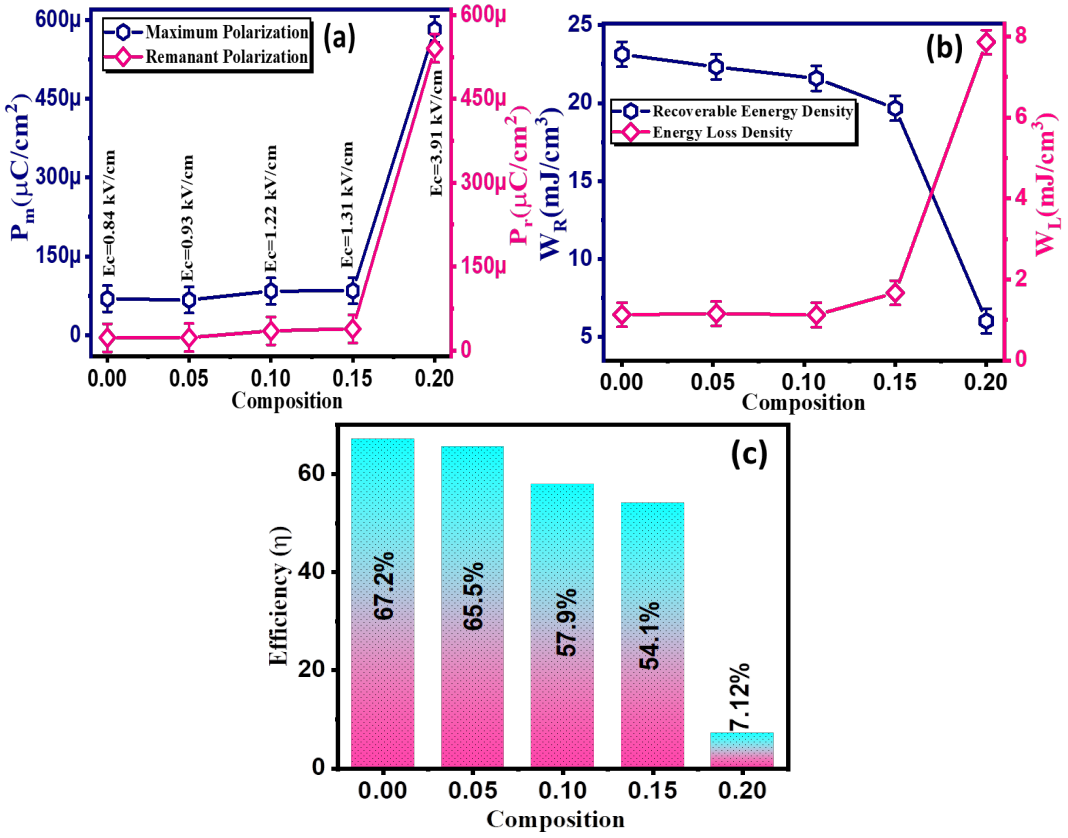

Fig. 7. (a) Maximum and remanent polarization, (b) recoverable and energy loss density and (c) energy storage efficiency of La/Cr co-doped $BiFeO_3$.

Table 5. Computed P_s, E_c and P_r for $Bi_{0.9}La_{0.1}Fe_{1-x}Cr_xO_3$ (x = 0, 0.05, 0.10, 0.15 & 0.20).

Sample Composition	P_{max} (μC/cm^2)	E_c (volt)	P_r (μC/cm^2)
$La_{0.1}Bi_{0.9}FeO_3$	6.80×10^{-5}	1.45	2.31×10^{-5}
$La_{0.1}Bi_{0.9}Fe_{0.95}Cr_{0.05}O_3$	7.01×10^{-5}	1.52	2.42×10^{-5}
$La_{0.1}Bi_{0.9}Fe_{0.90}Cr_{0.10}O_3$	8.47×10^{-5}	1.84	3.64×10^{-5}
$La_{0.1}Bi_{0.9}Fe_{0.85}Cr_{0.15}O_3$	8.55×10^{-5}	1.97	4.01×10^{-5}
$La_{0.1}Bi_{0.9}Fe_{0.80}Cr_{0.20}O_3$	5.90×10^{-4}	4.09	5.50×10^{-4}

The charge storage capability of a material decreases due to a decrease in permittivity because of high porosity and so higher density increases the permittivity of the material consequently upsurging its ferroelectric response [4, 61]. The conclusion to minimize the leakage problems associated with BFO-based ceramics is to produce denser and phase-pure microstructures. The reason for this improved ferroelectric behavior is the larger number of electric dipoles per unit volume (polarization) in a denser medium as compared to a porous one. Further, the replacement of La at Bi and Cr at Fe site decreases O vacancy concentration which reduces leakage current density due to refinement in domain pinning effects and upgrades the polarization [3, 4, 48, 51]. Ferroelectricity in BFO differs from other perovskite material in the sense that a lone pair of electrons interact with p electrons of oxygen causing off-centering displacement within the cationic environment which results in the formation of the localized lobe. This structural modification can also originate the ferroelectricity in BFO [4, 24, 53, 62]. From the calculated P_M, $P_{R,}$ and E_C values, the recoverable energy density and energy loss density were calculated and presented in Figure 7(b). These calculations lead to the computation of energy storage efficiency of these materials which is plotted against composition in Figure 7(c). It has been observed that though incorporation of La and Cr stabilized and crystal structure, reduced oxygen vacancy and leakage current but suppressed the energy storage efficiency of the material as well.

4. Conclusion

Here we synthesized $La_{0.1}Bi_{0.9}Fe_{1-x}Cr_xO_3$ (x = 0, 0.05, 0.10, 0.15, and 0.20) NPs utilizing the well-known and economical sol-gel auto-combustion approach to analyze its structural, magnetic and ferroelectric response. The incorporation of La and Cr did not affect the crystal symmetry of the parent composition however, lattice parameters were reduced depending on the relative ionic radius of the host and dopant. The calculation values of different profile factors from Rietveld's refinement assured the credibility of the developed crystal structure. The maximum value of Mr was noticed as 4.9142×10^{-3} emu/g for $La_{0.1}Bi_{0.9}Fe_{0.85}Cr_{0.15}O_3$ which was 47 times higher than the parent composition. The ferroelectric analysis revealed and significant improvement and $La_{0.1}Bi_{0.9}Fe_{0.80}Cr_{0.20}O_3$ exhibited the P_R is 5.50×10^{-4} μC/cm^2 which is 24 times higher than the first composition. It is claimed that altering a material's microstructure beyond a specific doping limit will reduce its performance. Therefore, this co-doping approach is believed to pave the path for BFO-based compositions for futuristic technological devices.

Acknowledgments

Researchers Supporting Project number (RSP2024R397), King Saud University, Riyadh, Saudi Arabia

References

[1] O. Singh, A. Agarwal, S. Sanghi, A. Das, others, J. Magn. Magn. Mater. 426, 369 (2017); https://doi.org/10.1016/j.jmmm.2016.11.109

[2] W. Hu, Y. Chen, H. Yuan, G. Zhang, G. Li, G. Pang, S. Feng, J. Solid State Chem. 183,1582 (2010); https://doi.org/10.1016/j.jssc.2010.04.041

[3] M. Amin, H. M. Rafique, M. Yousaf, S. M. Ramay, S. Atiq, J. Mater. Sci. Mater. Electron. 27, 11003 (2016); https://doi.org/10.1007/s10854-016-5216-8

[4] M. Amin, H. M. Rafique, M. Yousaf, S. M. Ramay, M. Saleem, S. K. Abbas, S. Atiq, J. Mater. Sci. Mater. Electron.1 (2017); https://doi.org/10.1007/s10854-017-7654-3

[5] A. A. Amirov, I. K. Kamilov, D. M. Yusupov, L. A. Reznichenko, O. N. Razumovskaya, I. A. Verbenko, Phys. Procedia 75, 10 (2015); https://doi.org/10.1016/j.phpro.2015.12.002

[6] S. Atiq, M. Faizan, A. H. Khan, A. Mahmood, S. M. Ramay, & S. Naseem, Results in Physics 12, 1269 (2019); https://doi.org/10.1016/j.rinp.2019.01.011

[7] P. Verma, & P. K. Roy, J. Mater. Sci.: Mater. Electron. 31(16), 13028 (2020); https://doi.org/10.1007/s10854-020-03853-2

[8] A. H. Khan, S. Atiq, M. S. Anwar, S. Naseem, S. K. Abbas, J. Mater. Sci.: Mater. Electron. 29(14), 11812 (2018); https://doi.org/10.1007/s10854-018-9281-z

[9] E. Bousquet, & A. Cano, Phys. Sci. Rev. (2021); https://doi.org/10.1515/9783110582130-005

[10] P. Baettig, N. A. Spaldin, Appl. Phys. Lett. 86, 012505 (2005); https://doi.org/10.1063/1.1843290

[11] N. M. Murari, R. Thomas, A. Winterman, R. E. Melgarejo, S. P. Pavunny, R. S. Katiyar, J. Appl. Phys. 105, 084110 (2009); https://doi.org/10.1063/1.3116506

[12] Priyadharsini, A. Pradeep, C. Murugesan, P. M. Md Gazzali, G. Chandrasekaran, Combust. Sci. Technol. 186, 297 (2014); https://doi.org/10.1080/00102202.2013.859682

[13] A. Kumar, D. Varshney, Ceram. Int. 38, 3935 (2012); https://doi.org/10.1016/j.ceramint.2012.01.046

[14] F. Lin, Q. Yu, L. Deng, Z. Zhang, X. He, A. Liu, W. Shi, J. Mater. Sci. 52, 7118 (2017); https://doi.org/10.1007/s10853-017-0947-3

[15] M. Amin, H. M. Rafique, G. M. Mustafa, A. Mahmood, S. M. Ramay, S. Atiq, S. M. Ali, J. Mater. Res. Technol. 13, 1534 (2021); https://doi.org/10.1016/j.jmrt.2021.05.066

[16] J. Wei, D. Xue, Electrochem. Solid State Lett. 10, G85 (2007); https://doi.org/10.1149/1.2772412

[17] S.J. Kim, A.Y. Kim, J.S. Kim, C.I. Cheon, S.H. Han, H.G. Kim, J. Korean Phys. Soc. 56(12), 439 (2010); https://doi.org/10.3938/jkps.56.439

[18] J. Xu, D. Xie, C. Yin, T. Feng, X. Zhang, H. Zhao, G. Li, T.L. Ren, Y. Guan, X. Gao, W. Pan, Mater. Lett. 122, 139 (2014); https://doi.org/10.14361/transcript.9783839426593

[19] N.M. Deraz, J. Alloys Compd. 501, 317 (2010); https://doi.org/10.1016/j.jallcom.2010.04.096

[20] W. iu, G. Tan, X. Xue, G. Dong, H. Ren, A. Xia, Ceram. Int. 40,12179 (2014); https://doi.org/10.1016/j.ceramint.2014.04.058

[21] Q. R. Yao, J. Cai, H. Y. Zhou, G. H. Rao, Z. M. Wang, J. Q. DengJ. Alloys Compd. 633, 170 (2015); https://doi.org/10.1016/j.jallcom.2015.01.123

[22] A. S. Priya, I. S. Banu, M. Chavali, Arab. J. Sci. Eng. 40, 2079 (2015); https://doi.org/10.1007/s13369-015-1668-z

[23] E. Mostafavi, A. Ataie, Mater. Sci. Pol. 34, 148 (2016); https://doi.org/10.1515/msp-2016-0017

[24] Z. X. Cheng, A. H. Li, X. L. Wang, S. X. Dou, K. Ozawa, H. Kimura, S. J. Zhang, T. R. Shrout, J. Appl. Phys. 103, 07E507 (2008); https://doi.org/10.1063/1.2839325

[25] B. Wang, X. Tian, X. Song, L. Ma, S. Yu, C. Hao, K. Chen, Q. Lei, Colloids Surf. Physicochem. Eng. Asp. 461, 184 (2014); https://doi.org/10.1016/j.colsurfa.2014.07.046

[26] P. harma, V. Verma, J. Magn. Magn. Mater. 374, 18 (2015);

https://doi.org/10.1016/j.jmmm.2014.08.002
[27] M. K. Singh, W. Prellier, M. P. Singh, R. S. Katiyar, J. F. Scott, Phys. Rev. B 77,144403 (2008); https://doi.org/10.1103/PhysRevB.77.144403
[28] B. Ramachandran, M. R. Rao, Appl. Phys. Lett. 95, 142505 (2009); https://doi.org/10.1063/1.3242411
[29] B. Bhushan, Z. Wang, J. Tol, N. S Dalal, A. Basumallick, N. Y. Vasanthacharya, S. Kumar, D. Das, J. Am. Ceram. Soc. 95, 1985 (2012); https://doi.org/10.1111/j.1551-2916.2012.05132.x
[30] Y. Zhang, S. Yu, J. Cheng, J. Eur. Ceram. Soc. 30, 271 (2010); https://doi.org/10.1016/j.jeurceramsoc.2009.05.005
[31] W. Shatti, Z.M.A. Abbas, Z. Khodair, J. Ovonic Res. 18(4), 473-9 (2022). https://doi.org/10.15251/JOR.2022.184.473
[32] P. Godara, A. Agarwal, N. Ahlawat, S. Sanghi, R. Dahiya, J. Alloys Compd. 594, 175 (2014); https://doi.org/10.1016/j.jallcom.2014.01.103
[33] S. S. Arafat, Chin. Phys. B 23, 066101(2014); https://doi.org/10.1088/1674-1056/23/6/066101
[34] J. Wei, M. Zhang, H. Deng, S. Chu, M. Du, H. Yan, Ceram. Int. 41, 8665 (2015); https://doi.org/10.1016/j.ceramint.2015.03.079
[35] B. uo, H. Deng, X. Zhai, W. Zhou, X. Meng, G. Weng, S. Chen, P. Yang, J. Chu, Mater. Lett. 186, 198 (2017); https://doi.org/10.1016/j.matlet.2016.09.094
[36] Hussain T, Siddiqi SA, Atiq S, Awan MS. 2013, Prog. Nat. Sci. Mater. Int. 23:487-492; https://doi.org/10.1016/j.pnsc.2013.09.004
[37] M. S. Bernardo, Bol. Soc. Esp. Ceram. Vidr. 53, 1 (2014); https://doi.org/10.3989/cyv.12014
[38] S. T Zhang, Y. Zhang, M. H. Lu, C. L. Du, Y. F. Chen, Z. G. Liu, Y. Y. Zhu, N. B. Ming, X. Q. Pan, Appl. Phys. Lett. 88, 162901 (2006); https://doi.org/10.1063/1.2195927
[39] P. Baettig, N. A. Spaldin, Appl. Phys. Lett. 86, 012505 (2005); https://doi.org/10.1063/1.1843290
[40] J. Z. Huang, Y. Wang, Y. Lin, M. Li, C. W. Nan, J. Appl. Phys. 106, 063911 (2009); https://doi.org/10.1063/1.3225559
[41] S. Basu, S. K. M. Hossain, D. Chakravorty, M. Pal, Curr. Appl. Phys. 11, 976 (2011); https://doi.org/10.1016/j.cap.2010.12.034
[42] J. Yang, X. Li, J. Zhou, Y. Tang, Y. Zhang, Y. Li, J. Alloys Compd. 509, 9271 (2011); https://doi.org/10.1016/j.jallcom.2011.07.023
[43] V. A. Reddy, N. P. Pathak, R. Nath, J. Alloys Compd. 543, 206 (2012); https://doi.org/10.1016/j.jallcom.2012.07.098
[44] G. Dhir, P. Uniyal, N. K. Verma, J. Supercond. Nov. Magn. 27, 1569 (2014); https://doi.org/10.1007/s10948-014-2480-9
[45] C. Ederer, N. A. Spaldin, Phys. Rev. B 76, 214404 (2007); https://doi.org/10.1103/PhysRevB.76.214404
[46] Amin Muhammad, Exploring the multifunctional properties of BiFeO3-based multiferroics [Doctoral dissertation], Lahore, Pakistan: University of the Punjab; (2019)
[47] Y. Zhu, C. Quan, Y. Ma, Q. Wang, W. Mao, X. Wang, J. Zhang, Y. Min, J. Yang, W. Huang, Mater. Sci. Semicond. Process. 57, 178 (2017); https://doi.org/10.1016/j.mssp.2016.10.023
[48] N. Sharma, S. Kumar, A. K. Mall, R. Gupta, A. Garg, Mater. Res. Express 4, 015702 (2017); https://doi.org/10.1088/2053-1591/aa5579
[49] P. Tang, D. Kuang, S. Yang, Y. Zhang, J. Alloys Compd. 656, 912 (2016); https://doi.org/10.1016/j.jallcom.2015.10.010
[50] J. Rout, R. N. P. Choudhary, Phys. Lett. A 380, 288 (2016); https://doi.org/10.1016/j.physleta.2015.10.007
[51] A. Mukherjee, M. Banerjee, S. Basu, N. T. K. Thanh, L. A. W. Green, M. Pal, Phys. B Condens. Matter 448, 199 (2014); https://doi.org/10.1016/j.physb.2014.03.082
[52] S. R. Das, P. Bhattacharya, R. N. P. Choudhary, R. S. Katiyar, Effect of La substitution on

structural and electrical properties of BiFeO3 thin film, 99, 066107 (2006); https://doi.org/10.1063/1.2180451
[53] B. Dhanalakshmi, K. Pratap, B. P. Rao, P. S. Rao, J. Alloys Compd. 676, 193 (2016); https://doi.org/10.1016/j.jallcom.2016.03.208
[54] H. Ke, W. Wang, Y. Wang, J. Xu, D. Jia, Z. Lu, Y. Zhou, J. Alloys Compd. 509, 2192 (2011); https://doi.org/10.1016/j.jallcom.2010.09.213
[55] S. Attanayak, R. N. P. Choudhary, P. R. Das, Can. J. Phys. 92, 440 (2014); https://doi.org/10.1139/cjp-2013-0624
[56] J. G. Wu, Z. Fan, D. Q. Xiao, J. G. Zhu, J. Wang, others, Prog. Mater. Sci. 84, 335 (2016); https://doi.org/10.1016/j.pmatsci.2016.09.001
[57] J. Dho, X. Qi, H. Kim, J. L. MacManus-Driscoll, M. G. Blamire, J. Adv. Mater. 18(11), 1445 (2006); https://doi.org/10.1002/adma.200502622
[58] X. H. Xiao, J. Zhu, Y. R. Li, W. B. Luo, B. F. Yu, L. X. Fan, F. Ren, C. Liu, C. Z. Jiang, J. Appl. Phys. 40, 5775 (2007); https://doi.org/10.1088/0022-3727/40/18/039
[59] G. D. Hu, S. H. Fan, C. H. Yang, W. B. Wu, Appl. Phys. Lett. 92, 192905 (2008); https://doi.org/10.1063/1.2918130
[60] M. M. Kumar, V. R. Palkar, K. Srinivas, S. V. Suryanarayana, Appl. Phys. Lett. 76, 2764 (2000); https://doi.org/10.1063/1.126468
[61] R. Mazumder, D. Chakravarty, D. Bhattacharya, A. Sen, Mater. Res. Bull. 44, 555 (2009); https://doi.org/10.1016/j.materresbull.2008.07.017
[62] G. L. Yuan, S. W. Or, J. M. Liu, Z. G. Liu, Appl. Phys. Lett. 89(5), 052905 (2006); https://doi.org/10.1063/1.2266992